Induced crystallization and the physical properties of $PbO\text{-}Sb_2O_3\text{-}As_2O_3$: MoO_3 glass system

3.1 Introduction

The characteristics of glass ceramic depend on the kind and quantity of the crystal phase formed as well as on the residual glass composition. Hence, the selection of a suitable nucleating agent in the correct concentration and determination of the temperature and the time of nucleation and growth are important factors, in the formation of a glass ceramic. The nucleating agents that are generally used for controlled crystallization processes, giving rise to enormous numbers of nucleation centres in the original glass are, gold, silver, platinum or the oxides of Ti, Cr, Mn, Ce, V, Ni and Zr or certain sulfides or fluorides. Among various crystallizing agents, MoO_3 is expected to be more effective mineralizer especially in the glass systems like antimony-arsenate and expected to inculcate profound influence on the optical and electrical properties. Molybdenum oxide has already been used successfully as crystallization catalyst in a number of other glass systems [1].

Molybdenum oxide is an odour less white or slightly yellow to slightly bluish powder. In the gas phase, three oxygen atoms are double bonded to the central molybdenum atom. In the solid state, anhydrous MoO_3

is composed of layers of distorted MO_6 octahedra in an orthorhombic crystal. The octahedra share edges and form chains which are cross-linked by oxygen atoms to form layers. The octahedra have one short molydenum-oxygen bond to non-bridging oxygen [2].

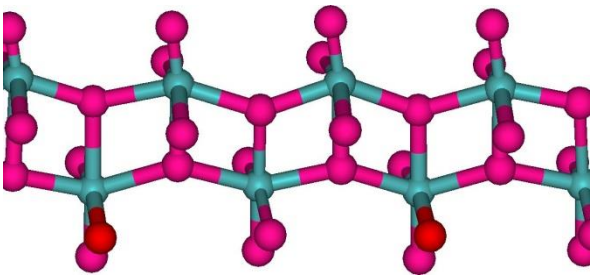

Fig. 3.1 MoO_3 structure

The image (Fig. 3.1) shows a section of the chain made up from edge sharing distorted octahedra. The oxygen atoms are above and below the chain link to other chains to build the layer. MoO_3 is used as a component of the co-catalyst used in the industrial production of acrylonitrile by the oxidation of propene and ammonia. Because of its layered structure and the ease of the Mo(VI)/Mo(V) couple, MoO_3 is of interest in electrochemical devices and displays [3].

MoO_3 based glasses have been the subject of many investigations due to their catalytic properties. The ions of molybdenum inculcate high activity and selectivity in a series of oxidation reactions of practical importance in the glass matrices [4, 5]. A considerable number of interesting studies are

available on the environment of molybdenum ion in various inorganic glasses [6-12]. Mo-O bond in molybdenum hexavalent oxide is identified as significantly covalent. The Mo ion exists in at least two stable valence states viz., Mo (V) and Mo (VI) and participate in the glass network with different structural units like MoO_4 (Td) and MoO_6 (Oh) of Mo^{6+} ions and $Mo^{5+}O^{3-}$ (Oh) of Mo^{5+} ions. In fact, earlier ESR studies on the glasses containing molybdenum ions have identified the presence of octahedrally coordinated Mo (V) ions along with distorted octahedrons approaching tetragons [13, 14]. These ions act both as network formers as well as network modifiers depending upon their concentration and nature of the host network. The Mo^{6+} ions are expected to participate in the glass network with tetrahedral MoO_4^{2-} structural units and may alternate with SbO_3 and AsO_3 structural units in MoO_3-As_2O_3-Sb_2O_3 glass matrix. A considerable number of studies are available on the understanding the structure of MoO_3 containing glasses by spectroscopic investigations [15-19] and ionic conductivity studies [20]. Few studies on the influence of molybdenum ions on dielectric properties of some glass systems are also available [21-25]. The presence of molybdenum ions makes the glasses to be useful for potential applications in high-density memories, light modulation; large area displays devices like smart windows and other electrochromic devices [26].

In this work, bulk crystallization of $PbO–Sb_2O_3–As_2O_3$ glasses in the presence of MoO_3 nucleant and the effect of the concentration of MoO_3 on the crystallization behavior and microstructure of glass ceramic products produced and their spectroscopic (optical absorption, ESR and IR), magnetic and dielectric properties have been investigated.

3.2 Brief review of the previous work on glasses and glass ceramics containing molybdenum ions

Yasser B Saddeek et al [27] have reported the synthesis and several features that include elastic properties and IR spectroscopic studies of the Na_2O-B_2O_3-Bi_2O_3-MoO_3 glasses. These results are interpreted in terms of the increase in the number of non-bridging oxygen atoms, substitution of longer bond lengths of Bi–O, and Mo–O in place of shorter B–O bond and the change in Na^+ ion concentration. Naoaki Kuwata et al [28] have studied cation dynamics of stabilized α-AgI in $AgI–Ag_2O–MoO_3$ glasses, by Ag-109 NMR spectroscopy. Their study has revealed that the silver ions in the type B composites transfer more smoothly across the interface between the α-AgI and the glass matrix than those in type A composite. Silvia et al [29] have investigated structural studies of $NaPO_3–MoO_3$ glasses by solid-state nuclear magnetic resonance and Raman spectroscopy. In their study it is found that structure is characterized by isolated phosphate species [most likely of the $P(OMo)_4$ type] and molybdenum oxide clusters with a large extent of Mo−O−Mo connectivity. Hemlata et al [30] have

reported characterization studies like X-ray absorption edge chemical shifts, infrared spectra and heat capacities of $AgI-Ag_2O-MoO_3$ glasses. They have discussed the probable anion structures in the oxygen excess and deficient regions. Al-Shukri et al [31] have studied electrical conductivity of molybdenum phosphate (MoO_3: P_2O_5) glasses. The electrical conductivity results for these glasses have been discussed using the small polaron model. El-Hofy and Hager [32] have measured ionic conductivity in MoO_3-BaF_2-AgI-LiF glasses. In their study it was found that at concentrations of LiF ≥10 mol%, an increased amount of Li^+ and F^- ions are weakly bound in interstitial positions among the basic constituting units MoO_6 and MoO_4. Jose Rajan et al [33] have reported the optical properties of MoO_3 containing tellurite glasses. In their study it was found that P_2O_5 generates $TeO_{5+\delta}$ groups in tellurite glasses that have a profound influence on their optical properties. Chung et al [34] have investigated the suitability of tellurite glasses modified with MoO_3 for ultra broad-band optical fibre amplifiers.

Iordanova et al [35] have studied the glass formation and structure of $PbO-B_2O_3$ glasses containing molybdenum ions by X-ray diffraction, differential thermal analysis and infrared spectroscopy; they have suggested the structural models for these glasses on the basis of IR spectral investigations and by comparing with known crystalline structures and showed that the glasses posses MoO_3 and MoO_6 groups as basic structural

units. Sekiya et al [36] have investigated molybdenum containing borate glasses by differential thermal analysis and Raman spectroscopy; they have concluded that the concentration of MoO_6 basic structural units depends on the contents of molybdenum ions in these glasses. Jamnicky et al [37] have reported the structure of Cu_2O-P_2O_5 glasses containing MoO_3 using infrared spectroscopy and concluded that the structure of these glasses depends strongly on composition of the glass matrix. Boudlich et al [38] have studied Mo^{5+} ions as EPR structural probe in phosphate glasses and their studies confirmed the distorted octahedral environment of MO^{5+} ions in these glasses.

El-Hofy and Hager [39] have studied ionic conductivity in MoO_3-BaF-AgI-LiF glasses and concluded that the basic glass constituting units are MoO_6 and MoO_4 structural groups. Machida [40] has investigated local environment of molybdenum ion in AgI-Ag_2O-MoO_3 glasses by NIR-FT Raman spectroscopy and FT-IR spectroscopy and showed that MoO_6 octahedra are linked to MoO_4 tetrahedra in these glasses. Bih et al [41] have reported the electrical properties of Na_2O-MoO_3-TeO_2 glasses. Muthupari and Rao [42] have performed thermal and infrared spectroscopic studies on Na_2O-P_2O_5 glasses doped with MoO_3 and proposed a structural model based on infrared spectroscopy. Qiu et al [43] have studied the electrical properties

of molybdenum containing Fe_2O_3-TeO_2 glasses; from these studies they have concluded that the electrical conduction of the glasses was due to small polaron hoping. Ingram et al [44] have investigated structural recovery in AgI-Ag_2O glasses containing molybdenum oxide by differential scanning calorimetry. Khattak et al [45] have reported the structure of molybdenum phosphate glasses by X-ray photoelectron spectroscopy and proposed a structural model basing on the amount of Mo^{6+} reduced to Mo^{5+}.

Though, a considerable number of studies on some MoO_3 glasses and glass ceramics are available, still there is a lot of scope to investigate the role of molybdenum ions on the structural aspects of lead antimony arsenate glass ceramics and their influence on physical properties

For the present study, a particular composition 40 PbO–(20-*x*) Sb_2O_3–40As_2O_3: *x* MoO_3 with six values of *x* ranging from 0 to 1.0 is chosen. The detailed compositions (all in mol%) are as follows:

M_0: 40 PbO- 20 Sb_2O_3- 40 As_2O_3

M_2: 40 PbO- 19.8 Sb_2O_3-40 As_2O_3: 0.2 MoO_3

M_4: 40 PbO- 19.6 Sb_2O_3-40 As_2O_3: 0.4 MoO_3

M_6: 40 PbO- 19.4 Sb_2O_3-40 As_2O_3: 0.6 MoO_3

M_8: 40 PbO- 19.2 Sb_2O_3-40 As_2O_3: 0.8 MoO_3

M_{10}: 40 PbO- 19.0 Sb_2O_3-40 As_2O_3: 1.0 MoO_3

The glass specimens with various concentrations of MoO_3 (prepared with the procedure described in Chapter 2) were heat treated for 6 h in a furnace at their crystallization temperatures Tc (340–360 ^oC), identified from differential thermal analysis of the glasses. Automatic controlling furnace was used to keep the temperature at the required level. After the heat treatment in the furnace at specified temperature, the samples were chilled in air to room temperature.

3. 3 Characterization

3.3.1 Scanning electron microscopy

Fig. 3.2 shows SEM pictures of the some of the PbO–Sb_2O_3–As_2O_3: MoO_3 glass ceramic samples; the pictures show an increasing crystallinity with increasing concentration of crystallizing agent MoO_3. The residual glass phase may be acting as interconnecting zones among the crystallized areas making the samples free of voids and cracks.

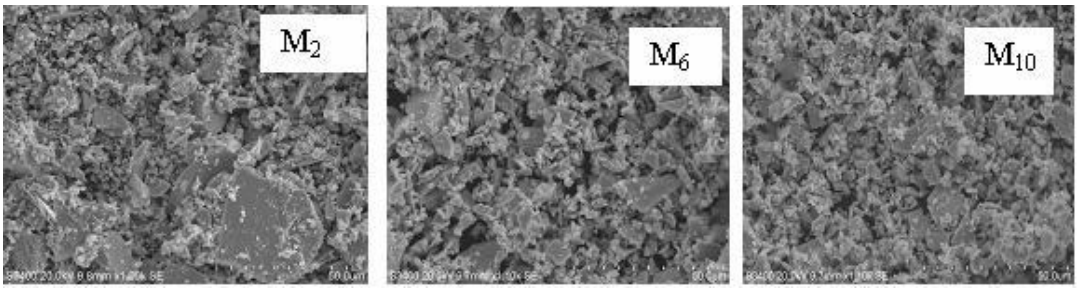

Fig 3.2 SEM images of some of the crystallized PbO-Sb_2O_3-As_2O_3: MoO_3 glass samples.

3.3.2 Energy dispersive spectroscopy and X-ray mappings

The chemical makeup of the glass ceramics is characterized by energy dispersive spectroscopy (EDS); The energy analysis of the glass ceramic materials indicates lead, arsenic, antimony and molybdenum elements in various crystalline phases (Fig. 3.3a). We have also recorded the X-ray maps of these glass ceramics for molybdenum ions (Fig. 3.3b)). The maps indicate the reasonably uniform distribution of molybdenum ions in the entire glass ceramic material. It may be noted here that the X-ray maps at different points were recorded even before the samples were crystallized. The maps appeared to be similar; hence, it may be taken it as granted as the distribution of Mo ions is uniform both in amorphous and crystalline phases.

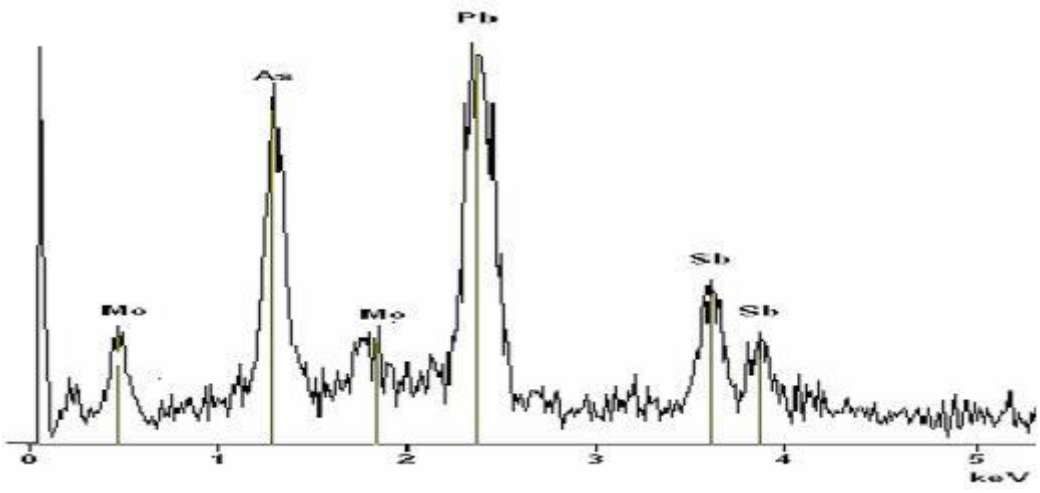

Fig 3.3(a) EDS spectra of one of the $PbO\text{-}Sb_2O_3\text{-}As_2O_3$: MoO_3 glass ceramic samples.

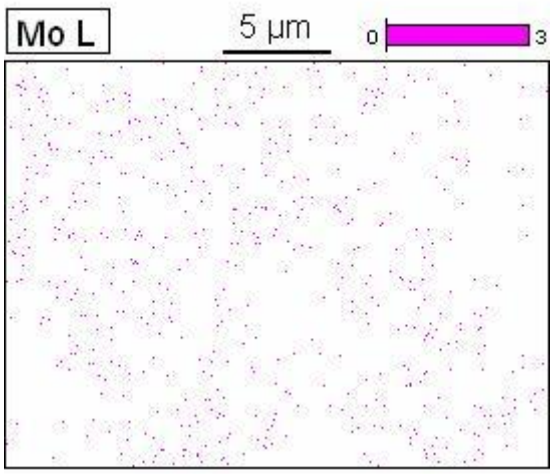

Fig. 3.3(b) X-ray mappings of molybdenum ions in one of $PbO\text{-}Sb_2O_3\text{-}As_2O_3$: MoO_3 glass ceramic samples.

3.3.3 X-ray diffraction

The X-ray diffraction analysis of the pre-heated PbO-Sb_2O_3-As_2O_3: MoO_3 glass samples shows that the samples prepared are of amorphous in nature. X-ray diffraction patterns of glass ceramic samples (Fig. 3.4) exhibit micro-structural changes. $Pb_5Sb_2O_8$, $PbSb_2O_6$, $SbAsO_4$, Sb_2MoO_6, $Sb_4Mo_{10}O_{31}$, $As_4Mo_3O_{15}$, $Pb_5Sb_4O_{11}$, that are kinetically and thermodynamically feasible seemed to be the main crystalline products in these samples (card numbers 22-0381, 49-1867, 01-0728, 33-1491, 33-0104, 41-0362 and 21-0941 respectively) [46]. The patterns indicate that antimony ions exist in Sb^{5+} oxidation state in addition to Sb^{3+} state especially in the samples M_2 and M_4. Similarly the crystalline phases of Mo^{5+} ions also detected in addition to Mo^{6+} compounds. The approximate fractions of Mo^{5+} ions that take part in the crystallization in each sample with respect to that of the sample M_{10} are evaluated from these XRD pattern; the values are found to be in the following order: M_2(55%), M_4 (67%), M_6 (79%), M_8 (91%).

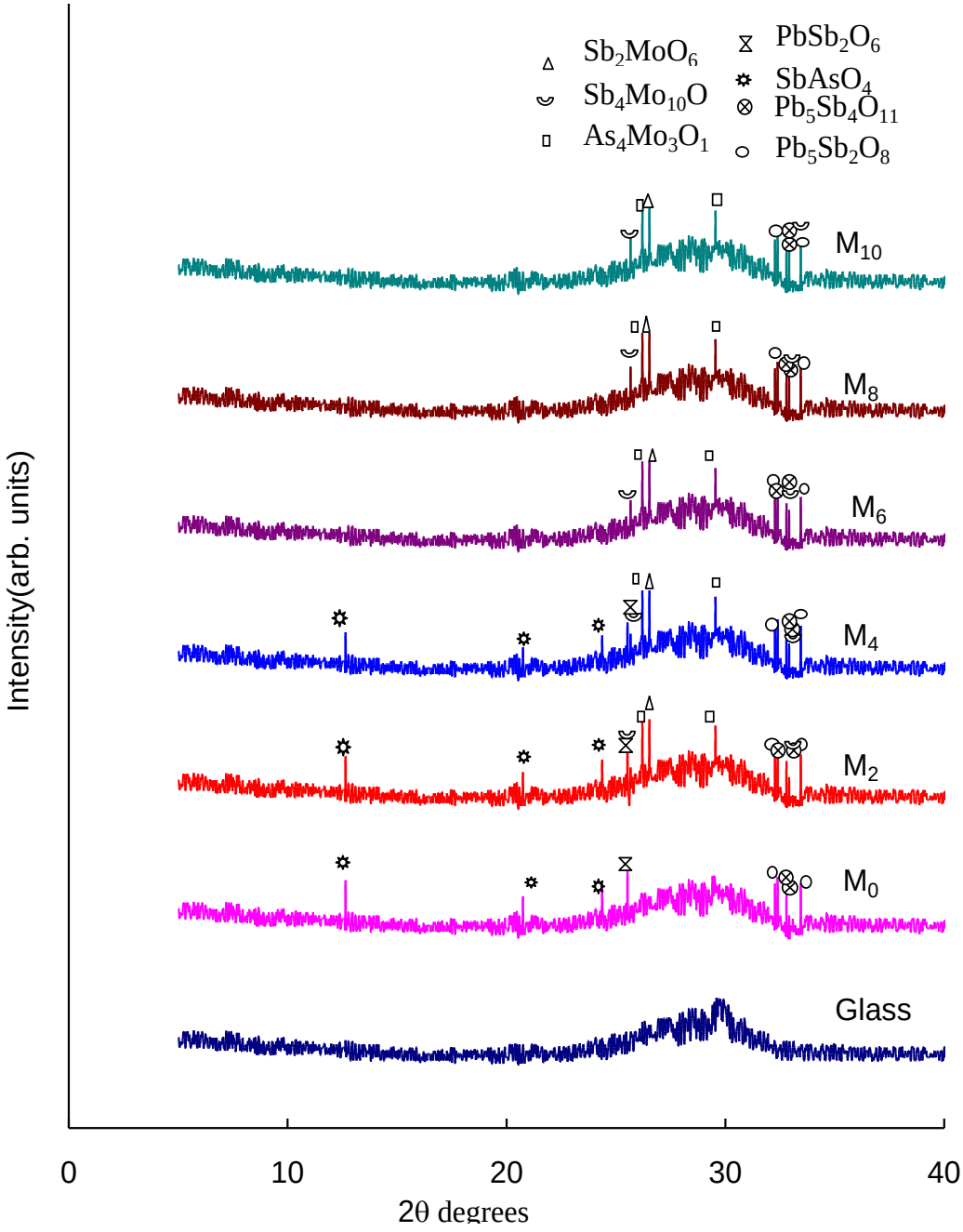

Fig 3.4. XRD patterns of PbO-Sb_2O_3-As_2O_3 glasses crystallized with different concentrations of MoO_3

3.3.4 Differential thermal analysis

Fig. 3.5 shows the differential thermal analysis traces of $PbO–Sb_2O_3–As_2O_3$: MoO_3 for some of the glass ceramic samples. For the pre-crystallized pure sample an endothermic change due to the glass transition temperature T_g is observed at about 255 ^oC. At still high temperature T_c an exothermic peak due to the crystal growth followed by another endothermic peak due to re-melting of the glass are also observed. The appearance of only one crystallization peak in the DTA traces of pre-crystallized samples indicates that the dopant, i.e., MoO_3, is homogeneously distributed in the material. DTA traces of all the crystallized samples exhibited an endothermic change due to the glass transition between 240 and 260 ^oC. In addition two clear exothermic peaks T_{C1}, T_{C2} due to the crystal growth followed by an endothermic peak due to re-melting of the samples have been observed. As the concentration of MoO_3 is increased the two exothermic peaks are merged into a single broad peak.

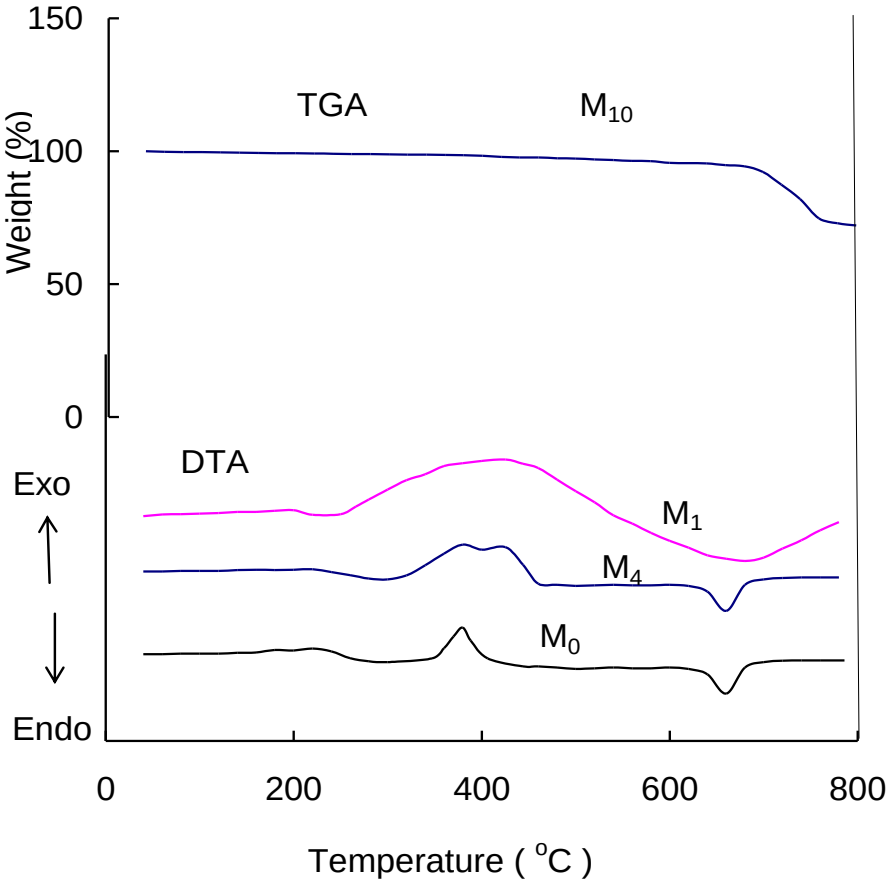

Fig. 3.5 TGA and DTA traces of some of PbO- Sb_2O_3-As_2O_3: MoO_3 glass ceramic samples.

3.3.5 Physical parameters

The density of the MoO_3 free glass material is measured to be 5. 727 g/cm^3. The gradual increase of MoO_3 in the glass matrix caused a slight decrease in the density; a similar trend is continued when the glasses are crystallized. However, the density of each ceramic sample is observed to be considerably higher than that of corresponding glass sample (Table 3.1). From the measured values of the density and average molecular weight $\overline{M}$

of the samples, various other physical parameters such as molybdenum ion concentration N_i, mean molybdenum ion separation r_i, polaron radius r_p in PbO- Sb_2O_3-As_2O_3: MoO_3 glass-ceramics are computed and presented in Table 3.1.

Table 3.1
Various physical properties of PbO- Sb_2O_3-As_2O_3: MoO_3 glass ceramics.

Glass-ceramics	M_0	M_2	M_4	M_6	M_8	M_{10}
Density d (gm/cm^3)	5.7904 (5.727)	5.7654 (5.717)	5.7572 (5.707)	5.7533 (5.698)	5.7501 (5.686)	5.7467 (5.677)
Average molecular weight $\overline{M}$	226.7	226.4	226.13	225.8	225.5	225.2
Mo^{6+} ion conc. N_i (10^{21} ions/cm^3)	-	3.07	6.13	9.21	12.3	15.4
Inter – ionic distance c Mo ions r_i (A^o)	-	6.88	5.46	4.77	4.33	4.02
Polaron radius (A^o) r_p	-	2.77	2.2	1.92	1.75	1.62

* The density value given in the parenthesis is the density of corresponding glass sample

3.4 Results

3.4.1 IR spectra

IR spectrum of crystalline Sb_2O_3 exhibited four fundamental absorption bands designated by ν_1 (925 cm^{-1})—due to symmetric stretching vibrations, ν_2 (600 cm^{-1})—due to symmetric bending vibrations, ν_3 (710 cm^{-1})-due to doubly degenerate stretching vibrations and ν_4 (485 cm^{-1})—due to

doubly degenerate bending vibrations (ν_4) of SbO_3 structural units as was reported earlier [47, 48]. In the infrared spectrum of glass ceramic sample M_0, the band due to ν_1 vibrations of SbO_3 structural groups is observed at about 939 cm^{-1} and the band related to ν_2 vibrations of these units is observed at 617 cm^{-1}. The IR spectrum of crystalline As_2O_3 has also exhibited four fundamental absorption bands at ν_1 (1050 cm^{-1}), ν_2 (618 cm^{-1}), ν_3 (795 cm^{-1}) and ν_4 (505 cm^{-1}) [47]. In the spectrum of glass ceramic M_0, the ν_1 band as appeared at 1040 cm^{-1}, where as, the ν_2 bands and the ν_3 bands of SbO_3 and AsO_3 structural groups are merged and exhibited common meta-centres at 617 and 765 cm^{-1}, respectively. In the region of ν_4 vibrations, it is believed that the vibrations due to PbO_4 structural groups could be present; in fact the vibrational band due to PbO_4 units was reported at 470 cm^{-1} in a number of other glass systems [49].

After the crystallization with MoO_3, two new bands have appear at 890 and 835 cm^{-1} in the spectrum of glass ceramic M_2; these bands have been attributed to ν_1 and ν_3 vibrational modes of MoO_4^{2-} tetrahedral units respectively [50, 51]. With the rise in the concentration of the crystallizing agent, the intensity of the bands due to MoO_4^{2-} (ν_1) tetrahedral units is observed to decrease and is found to be shifted towards slightly higher

frequency side whereas the v_3 vibrational band is observed to be shifted towards lower frequency. Further, the intensity of bands due to symmetric

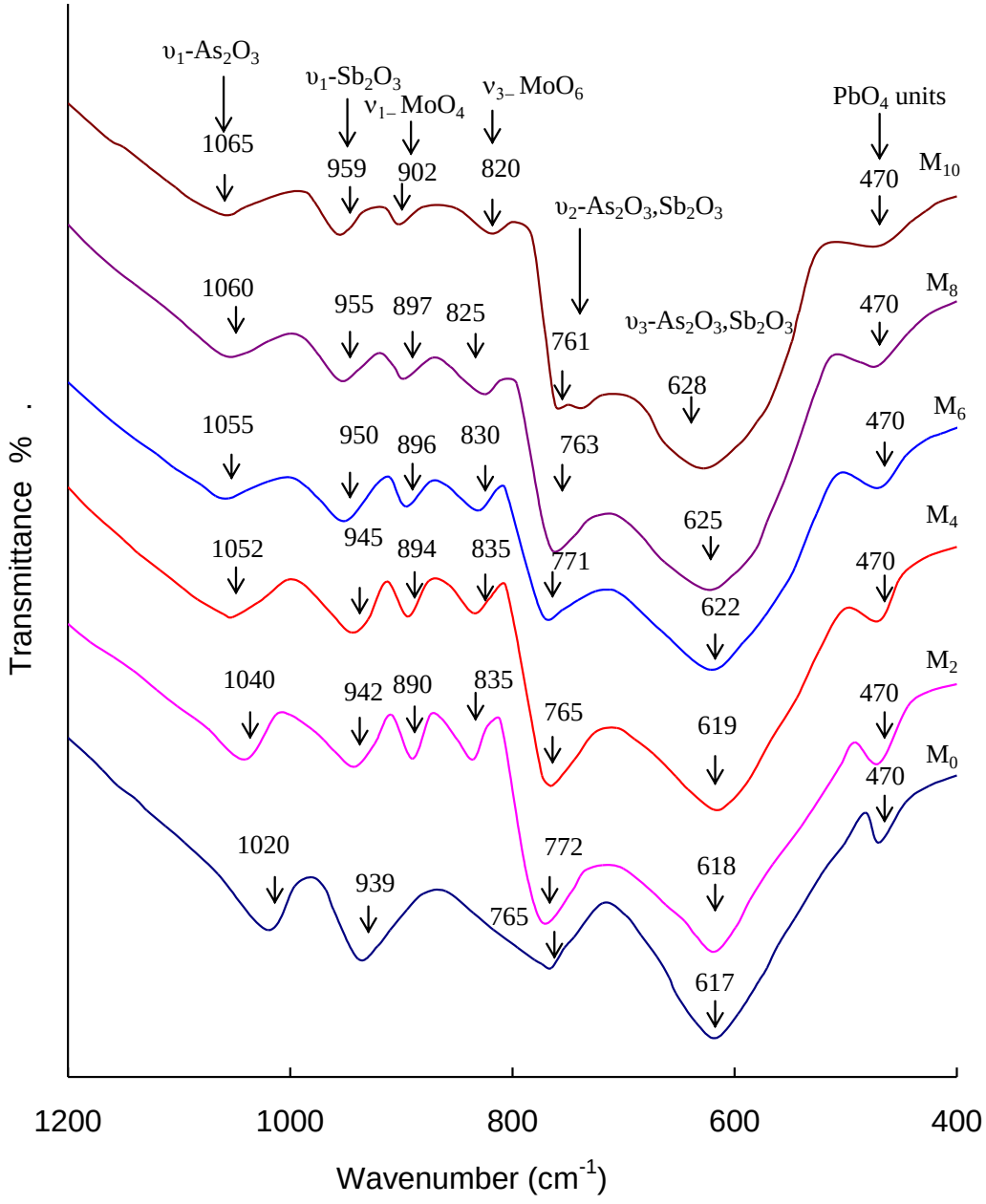

Fig 3.6 IR spectra of PbO-Sb_2O_3-As_2O_3: MoO_3 glass ceramic samples.

stretching and symmetric bending vibrations of SbO_3 and AsO_3 structural groups is also observed to decrease gradually with increase in the concentration of nucleating agent (Fig 3.6). The summary of the data on peak positions of various structural units in the IR spectra is furnished in Table 3.2.

Table 3.2

Summary of the data on the positions of the bands in IR spectra of PbO-Sb_2O_3-As_2O_3: MoO_3 glass ceramics.

Glass-ceramic	As_2O_3 Sb_2O_3		As_2O_3 / Sb_2O_3		MoO_4 groups		PbO_4 (cm^{-1})
	ν_1 (cm^{-1})		ν_2 (cm^{-1})	ν_3 (cm^{-1})	ν_3 (cm^{-1})	ν_1 (cm^{-1})	
M_0	1020	939	617	765	--	--	470
M_2	1040	942	618	772	835	890	470
M_4	1052	945	619	765	835	894	470
M_6	1055	950	622	771	830	896	470
M_8	1060	955	625	763	825	897	470
M_{10}	1065	959	628	761	820	902	470

3.4.2 Optical absorption spectra

Fig. 3.7 represents the optical absorption spectra of $PbO–Sb_2O_3$-As_2O_3: MoO_3 glass ceramic samples recorded at room temperature in the wavelength region 300-850 nm. The absorption edge observed at 382.5 nm for the glass ceramic sample M_0 is found to be shifted gradually towards higher wavelength with increase in the concentration of nucleating agent viz., MoO_3. Additionally, the spectra of the samples show a broad absorption band in the region 670-690 nm; there is a noticeable increase in the intensity of this band with a considerable shift of the meta centre towards the higher wavelength increase in the concentration of crystallizing agent. From the observed absorption edges, we have evaluated the optical band gaps (E_o) of these glass ceramics by drawing Urbach plot [51]. The value of optical band gap is found to decrease gradually with increase in the concentration nucleating agent (Fig.3.8, Table 3.3).

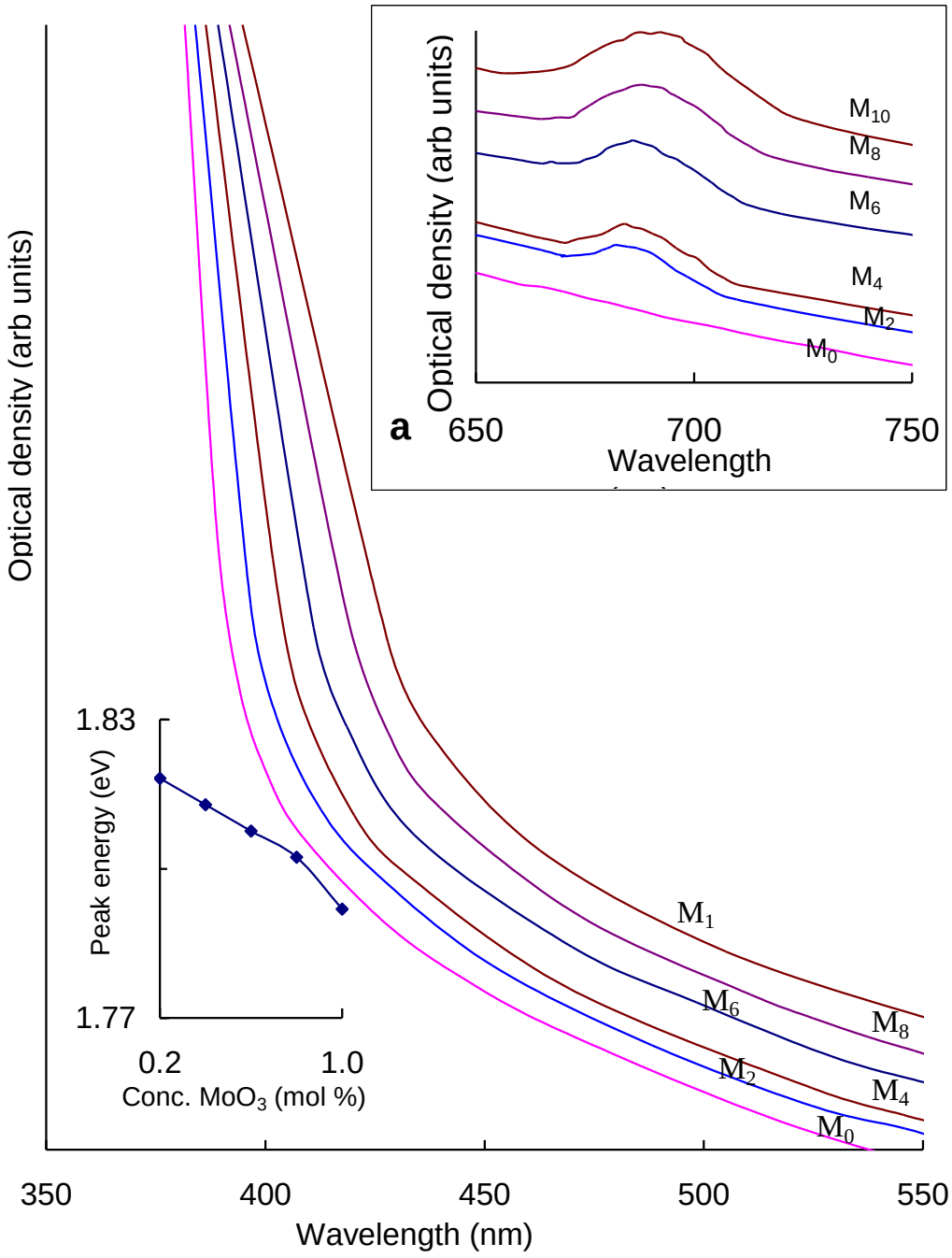

Fig 3.7 Optical absorption spectra of PbO-Sb_2O_3-As_2O_3 glass ceramics recorded at room temperature. Inset (a) represents the spectra recorded in the wavelength region of 650-750 nm and (b) gives the variation of peak energy with the concentration of MoO_3

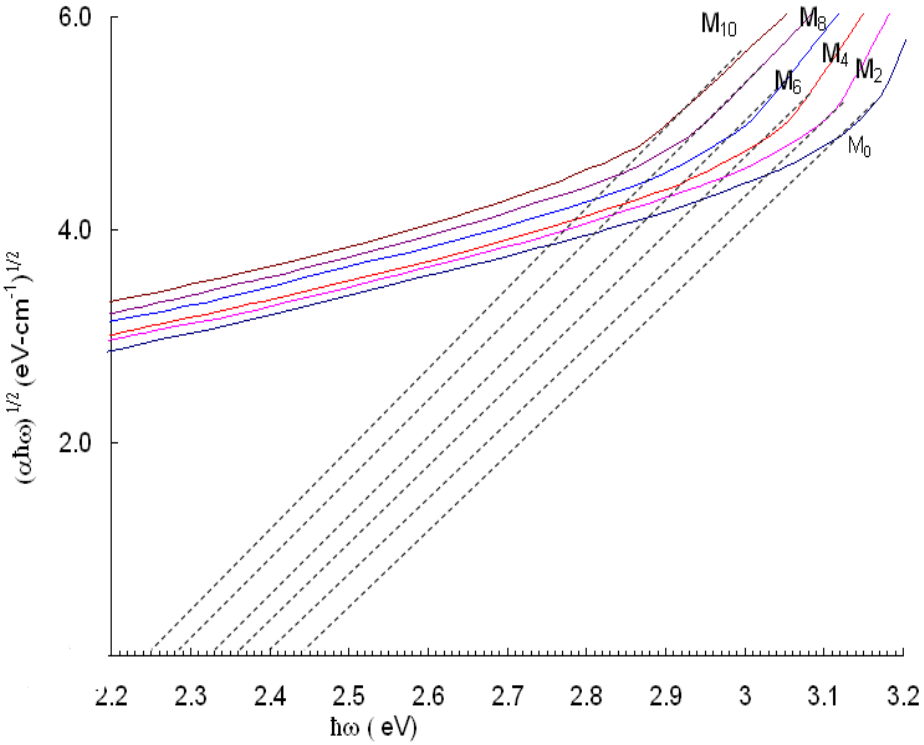

Fig. 3.8 Plots to evaluate optical band gaps for PbO-Sb_2O_3-As_2O_3: MoO_3 glass ceramics

Table 3.3

Summary of data on optical absorption spectral data of PbO-Sb_2O_3-As_2O_3: MoO_3 glass ceramics

Glass ceramic	Cut-off wavelength	Optical band gap E_o (eV)	Band position (nm)
M_0	381.6	2.44	-
M_2	384	2.39	682
M_4	386.4	2.36	684
M_6	389.2	2.33	686
M_8	391.8	2.29	688
M_{10}	394.8	2.25	692

3.4.3 ESR spectra

Fig. 3.9 shows the ESR spectra of $PbO\text{-}Sb_2O_3\text{-}As_2O_3$: MoO_3 glass ceramics recorded at room temperature. The spectra exhibit a signal consisting of an intense central line surrounded by smaller satellites (at $g_\perp \sim 1.933$ and $g_{ll} \sim 1.883$). The intensity of the signal is observed to increase with the gradual increase in the concentration of crystallizing agent MoO_3; the variation of half width $\Delta B_{1/2}$ of the signal with the concentration of the crystallizing agent is presented as the inset (a) of Fig. 3.9. The values of $g_\perp$ and g_{ll} are also observed to be dependent on the concentration of the crystallizing agent (Table 3.4).

Table 3.4

Data on and magnetic properties of $PbO\text{-}Sb_2O_3\text{-}As_2O_3$: MoO_3 glass ceramics.

Glass ceramic	g_{ll}	$g_\perp$	$\Delta B_{1/2}$ (mT)	d(nm)	χ (10^{-6}, emu)	C = N'/N_i	$\alpha = \frac{g_e - g_{ll}}{4(g_e - g_\perp)}$
M_2	1.889	1.909	5.44	1.25	9.12	0.15	0.352
M_4	1.891	1.912	5.79	1.31	19.41	0.16	0.365
M_6	1.892	1.913	5.9	1.44	38.29	0.21	0.370
M_8	1.895	1.914	6.03	1.49	56.01	0.23	0.375
M_{10}	1.896	1.915	6.5	1.67	91.46	0.30	0.382

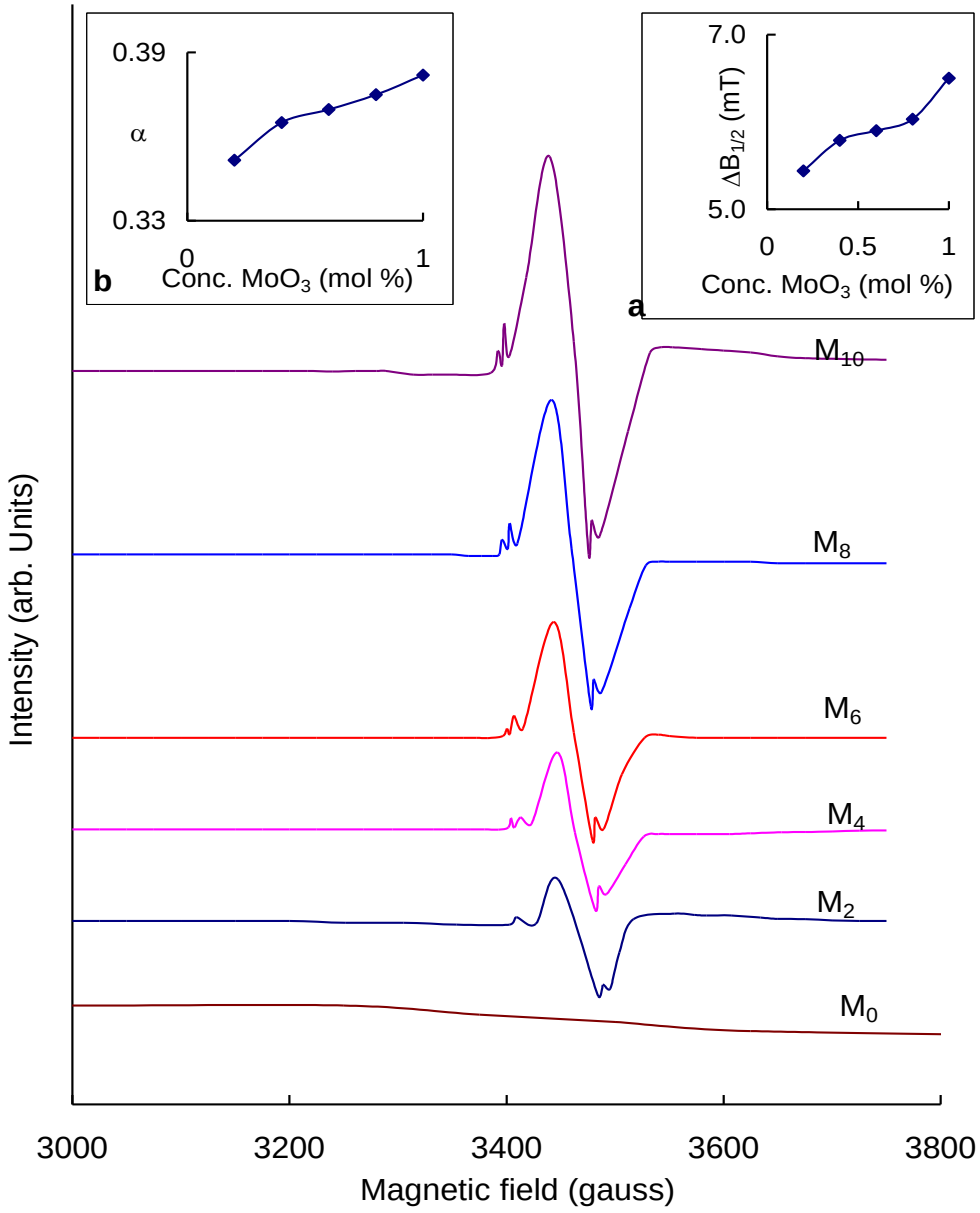

Fig.3.9 ESR spectra of PbO-Sb_2O_3-As_2O_3 glasses crystallized with different concentrations of MoO_3. Insets give the variation of (a) $\Delta B_{1/2}$ and (b) distortion parameter a, with the concentration of MoO_3

3.4.4 Magnetic susceptibility

The magnetic susceptibility measurements were also undertaken for these glass ceramic samples at room temperature and the values of χ obtained are presented in Table 3.4; the value of χ is found to increase gradually with the increase in the concentration of MoO_3. From the measured values of χ, the concentration of Mo^{5+} ions (N') is estimated by taking the value of magnetic moment as 1.7 μ_B. The ratio (C), N_i' total molybdenum ion concentration (N_i)/molybdenum ion concentration *N*i, is estimated from the values of N_i' and is furnished in the Table 3.4; the value of C is observed to increase significantly with increase in the concentration of crystallizing agent.

3.4.5 Dielectric properties

The dielectric constant ε' and loss tan δ at room temperature ($\approx$ 30 ^oC) of PbO- Sb_2O_3-As_2O_3 glass ceramic at 100 kHz are measured to be 14.7 and 0.005 respectively; these values are found to increase considerably with decrease in frequency. Fig. 3.10 represents the variation of dielectric constant and loss with frequency at room temperature of PbO-Sb_2O_3-As_2O_3 glasses crystallized with different concentrations of MoO_3; inset of the same figure shows the variation of these parameters with the concentration of

crystallizing agent MoO_3 measured at 1 kHz. The parameters, ε' and tanδ are observed to increase with the concentration of MoO_3.

The temperature dependence of ε' at 1 kHz of PbO- Sb_2O_3-As_2O_3 glasses crystallized with different concentrations of MoO_3 is shown in Fig. 3.11 and at different frequencies of glass ceramic sample M_4 is shown as the inset. The value of ε' is found to exhibit a considerable increase at higher temperatures especially at lower frequencies; however the rate of increase of ε' with temperature is found to increase with increase in the concentration of crystallizing agent.

A comparison plot of variation of tan δ with temperature, measured at a frequency of 10 kHz for all the glass ceramic samples is presented in Fig. 3.12. The inset of this figure represents the temperature dependence of tan δ of sample M_6 at different frequencies. The dependence of dielectric loss with temperature at different frequencies exhibits distinct maxima indicating dipolar relaxation character of dielectric loss in these glass ceramic samples. From these curves, it is also observed that the region of relaxation shifts towards lower temperatures (with broadening of relaxation peaks and increasing value of $(\tan \delta)_{max}$ with increase in the concentration of the nucleating agent. The effective activation energy W_d for the dipoles is

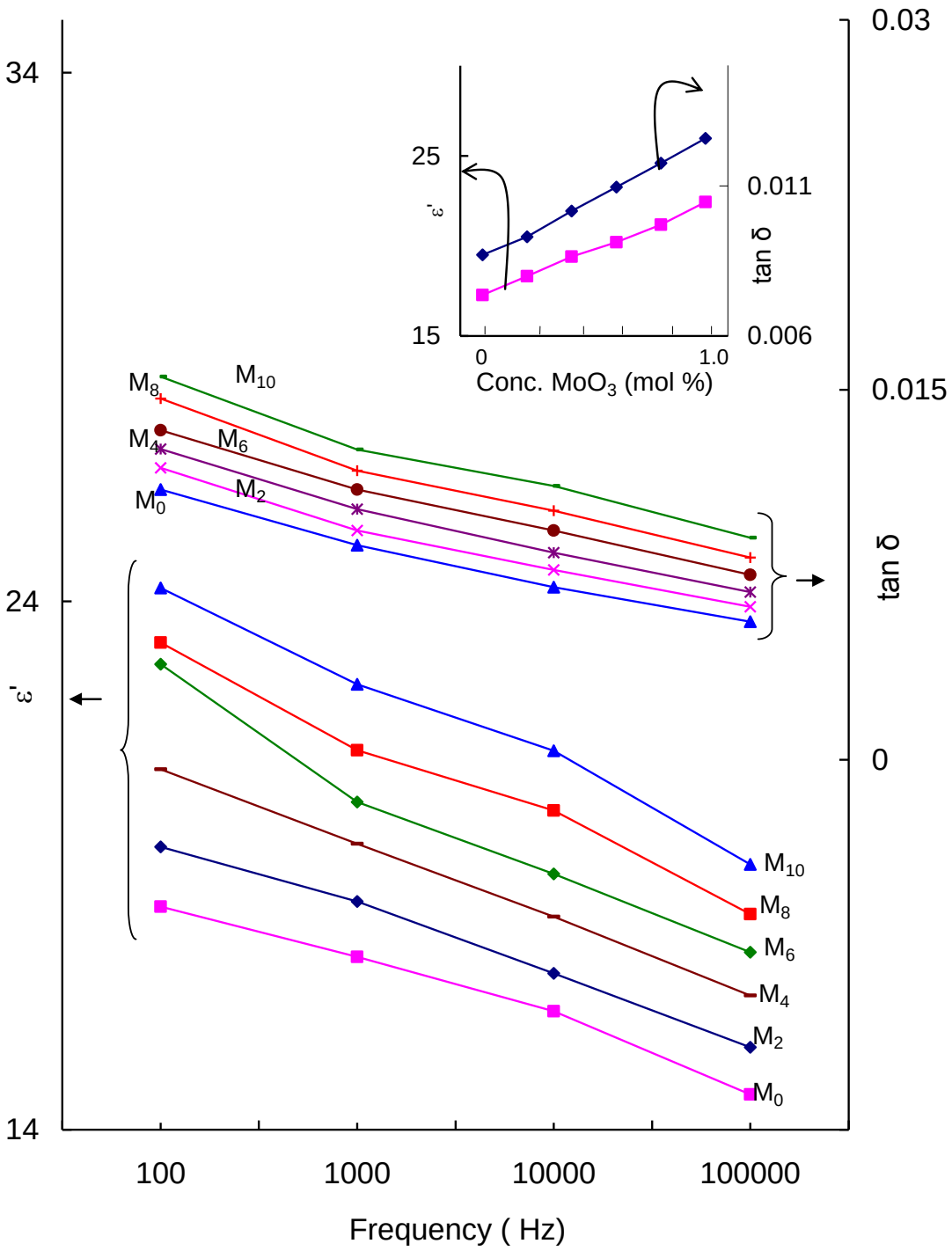

Fig. 3.10 Variation of dielectric constant and loss with frequency of PbO-Sb_2O_3-As_2O_3 glasses crystallized with different concentrations of MoO_3 measured at room temperature. Inset represents the variation of dielectric constant and loss at room temperature with the concentration of the crystallizing agent.

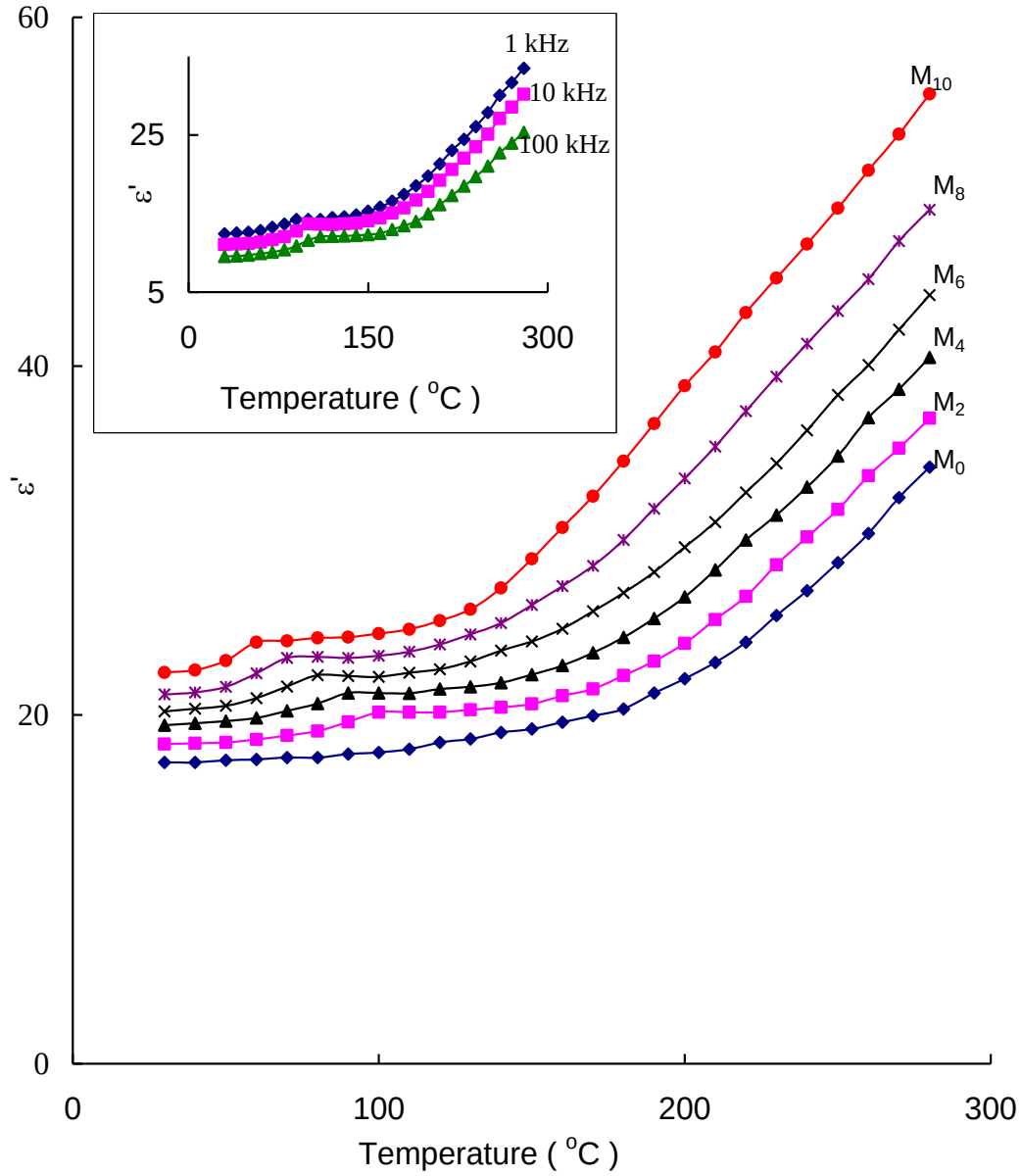

Fig.3.11 A comparison plot of variation of dielectric constant with temperature at 1 kHz for $PbO\text{-}Sb_2O_3\text{-}As_2O_3$: MoO_3 glass-ceramic. Inset gives the variation of dielectric constant with temperature at different frequencies of glass ceramic M_4.

evaluated for all the glass ceramic samples using the relation

$$f = f_o e^{-W_d / kT} \qquad \textbf{(3.1)}$$

and its variation with the concentration of MoO_3 is shown as inset (b) of Fig. 3.12; the activation energy is found to decrease gradually with increase in the concentration of the crystallizing agent. The pertinent data related to dielectric loss of these glasses is presented in Table 3.5.

Table 3.5

Data on dielectric loss of $PbO\text{-}Sb_2O_3\text{-}As_2O_3$: MoO_3 glass ceramics.

Glass ceramic	$(\tan\delta)_{Max.Avg}$	Temp. region of relaxation (^oC)	A.E for dipoles (eV)
M_0	----	----	----
M_2	0.0111	100-120	2.79
M_4	0.0126	90-110	2.65
M_6	0.0139	80-103	2.51
M_8	0.0155	70-90	2.37
M_{10}	0.0167	60-80	2.23

The a.c. conductivity σ_{ac} is calculated at different temperatures, using the relation

$$\sigma_{ac} = \omega\varepsilon_o\, \varepsilon' \tan\delta \qquad (3.2)$$

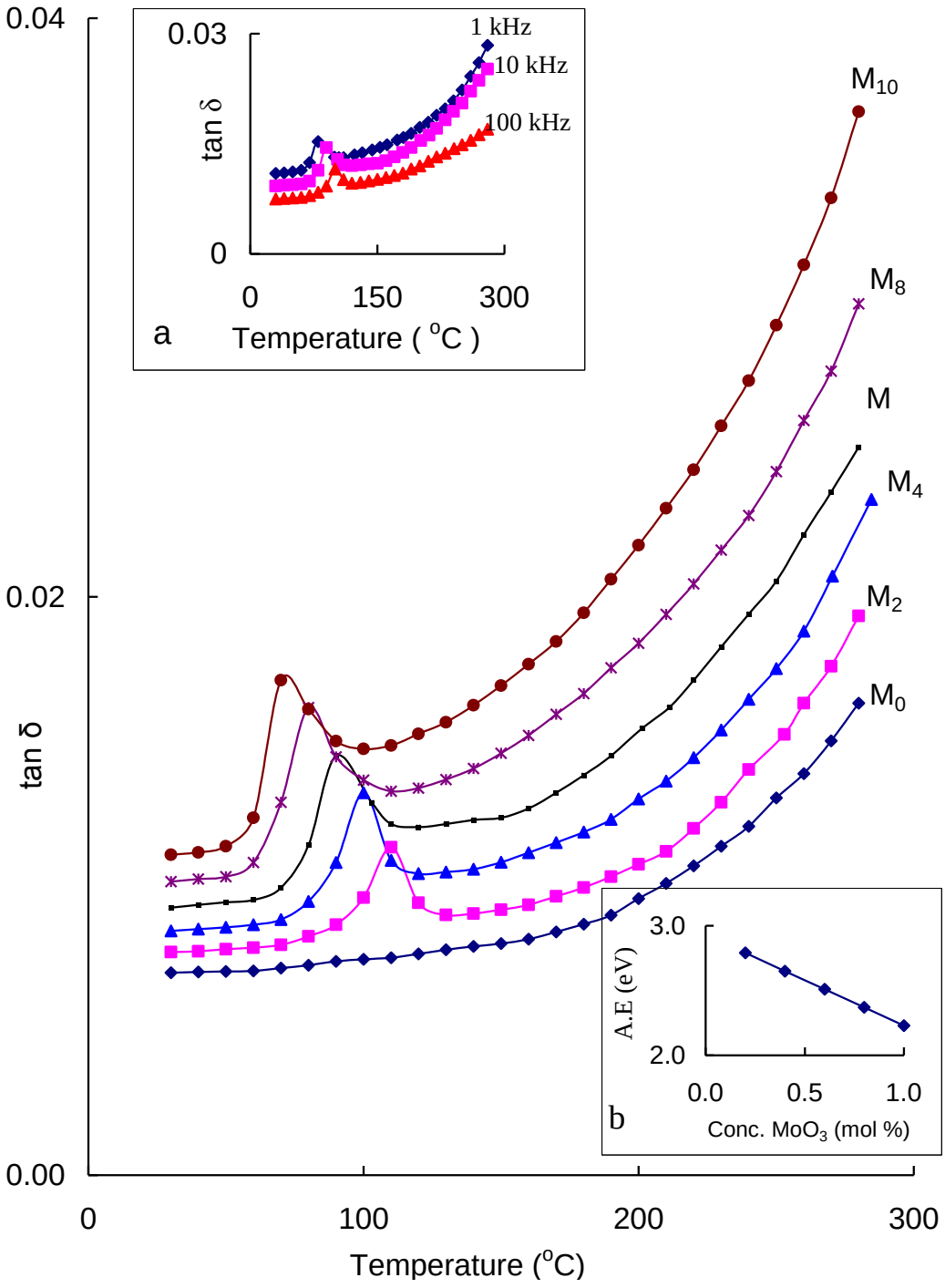

Fig. 3.12 A comparison plot of variation of dielectric loss with temperature at 10 kHz for $PbO\text{-}Sb_2O_3\text{-}As_2O_3$: MoO_3 glass-ceramics. Inset (a) gives the variation of dielectric loss with temperature at different frequencies of glass-ceramic M_6 and (b) gives the variation of activation energy of the dipoles with the conc. of the nucleating agent.

for different frequencies and the plots of log σ_{ac} against 1/T are shown in Fig 3.13 for all the glass ceramics at 100 kHz. From these plots, the activation energy for conduction in the high temperature region over which a near linear dependence of log σ_{ac} with 1/T could be observed is evaluated and presented in Table 3.6; this activation energy is also found to decrease gradually with increase in the concentration of the crystallizing agent.

Table 3.6
Summary of data on a.c. conductivity of $PbO\text{-}Sb_2O_3\text{-}As_2O_3$: MoO_3 glass ceramics

Glass	$N(E_F)$ in (10^{20}, eV^{-1}/cm^3)			A.E for conduction (eV)
	Austin and Mott	Pollak	Butcher and Hyden	
M_0	----	----	----	0.39
M_2	5.58	2.33	5.67	0.33
M_4	6.03	2.51	6.12	0.29
M_6	6.49	2.71	6.59	0.24
M_8	7.01	2.92	7.12	0.20
M_{10}	7.58	3.16	7.7	0.18

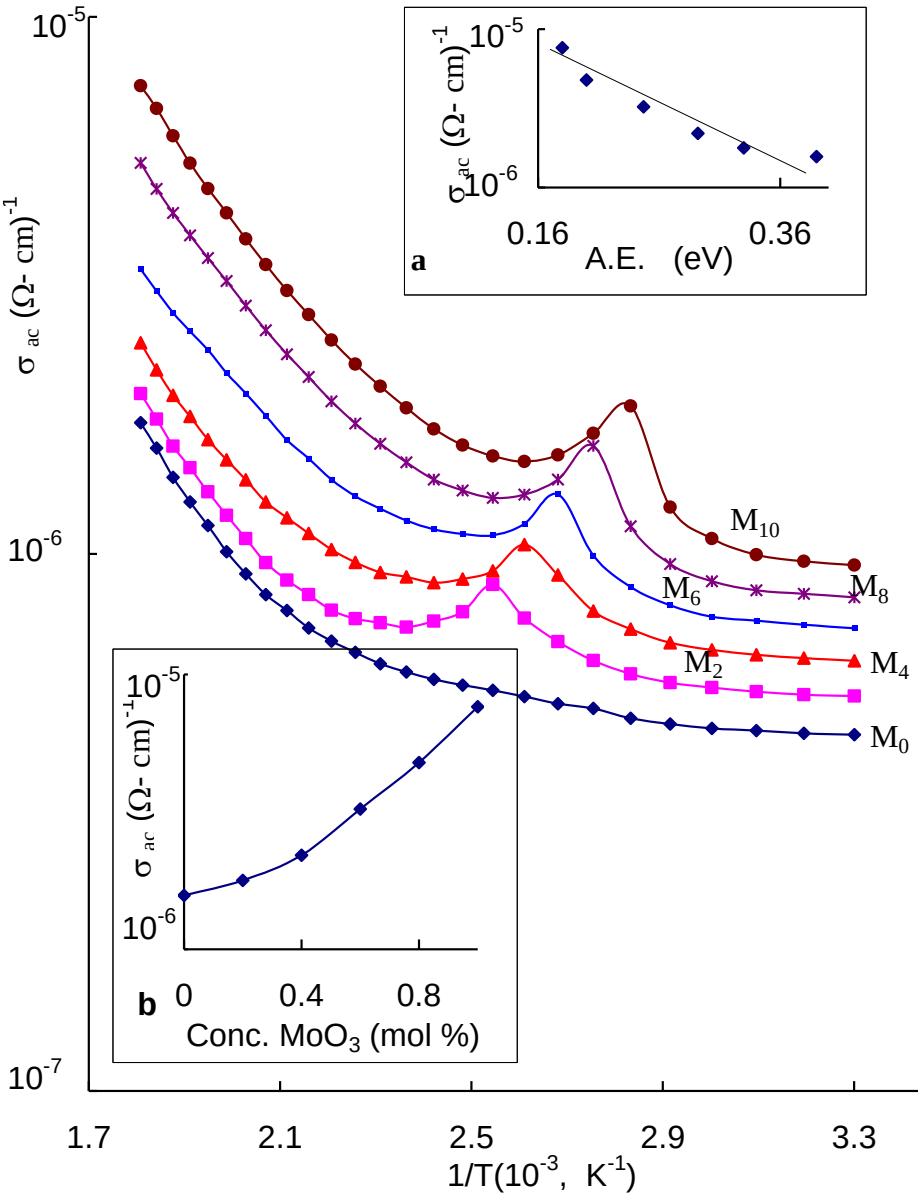

Fig. 3.13 Variation of s ac with 1/T at 100 kHz of $PbO\text{-}Sb_2O_3\text{-}As_2O_3$: MoO_3 glass ceramic. Inset (a) represents the variation of a.c. conductivity with activation energy for conduction for sample M_8. Inset (b) represents isotherm at 270 ^oC of σ_{ac} at 100 kHz, as a function of MoO_3 concentration.

3.5 Discussion

Among various constituents of $PbO\text{-}Sb_2O_3\text{-}As_2O_3$: MoO_3 glass-ceramics, Sb_2O_3 is a conditional glass former and it requires modifiers like PbO to form the glass.; it participates in the glass network with triangular SbO_3 pyramidal units as mentioned earlier. In the glass network, the Sb-O distances in SbO_3 units lie in between 2.0 and 2.6 Å with the coordination number of Sb as 3.0. The coordination polyhedra are joined by sharing corners to form double infinite chains with the lone pairs pointing out from the chains. These chains are held together by weak secondary Sb-O bonds with lengths greater than 2.6 Å. Further, the earlier X-ray diffraction investigations on some Sb_2O_3 glass systems indicated that the nearest neighbour Sb –Sb distance ~ 3.4 Å with the coordination number 1.7. The third oxygen in each SbO_3 units must take part in linkages of type Sb-O-As [52-55].

As_2O_3 is a strong network former with corner sharing AsO_3 pyramidal units; normal bond lengths of As-O lie in the range 1.72-1.81 Å and O-As-O and As-O-As bond angles lie in the range 90-103^o and 123-135^o, respectively [56, 57]. Further, there is a possibility for the cross linking of a part of SbO_3 units with As^{3+} ions to form Sb-O-As bonds in the glass network; this is reasonable because the ionic radii of As^{3+} (~ 0.70 Å) and Sb^{3+} (~ 0.90 Å)

are not very different from each other. The presence of common meta centers units of ν_2 and ν_3 vibrational bands in the ranges of 615 – 630 cm^{-1} and 760 - 775 cm^{-1} respectively of SbO_3 and AsO_3 structural units, in the IR spectra of the glass ceramics in fact supports such a view point. However, earlier EXAFS studies indicated that $Sb^{V}O_4$ units are more compatible in the network forming rather than SbO_3 trigonal pyramids units to form linkages with the conventional AsO_3 structural units [58]. The reasons are obvious; Sb^{3+} ion with its lone electron pair occupies a greater angular volume than a bonding pair of electrons. As a participant of glass network, the local structure of Sb^{3+} cations become less symmetric and the strain energy in the glass network increases as a whole, thus resulting in a decrease in the additional activation energy that is necessary for glass network rearrangement. As a result we expect that more degree of disorder in glasses containing Sb^{3+} ions rather than in the glasses containing Sb^{5+} ions.

PbO in general is a glass modifier and enters the glass network by breaking up the As-O-As, Sb-O-As bonds (normally the oxygens of PbO break the local symmetry while Pb^{2+} ions occupy interstitial positions) and introduces coordinate defects known as dangling bonds along with non-bridging oxygen ions. In this case the lead ions are octahedrally positioned to form octahedral units, Pb should be sp^3d^2 hybridized (6s, 6p and 6d orbitals)

[59, 60]. However, PbO may also participate in the glass ceramic network with PbO_4 structural units when lead ion is linked to four oxygens in a covalency bond configuration. Molybdenum ions are expected to exist mainly in the Mo^{6+} state in $PbO\text{-}Sb_2O_3\text{-}As_2O_3$: MoO_3 glass network. As the concentration of MoO_3 as crystallizing agent is increased, the color of the samples became increasingly brown, indicating the reduction of a part of molybdenum ions from Mo^{6+} state to Mo^{5+} state. These Mo^{5+} ions are quite stable and occupy octahedral positions with distortions due to the Jahn-Teller effect [60]. The Mo^{6+} ions participate in the glass network with tetrahedral MoO_4^{2-} structural units and may form the linkages with SbO_3 and AsO_3 structural units. Thus, $PbO\text{-}Sb_2O_3\text{-}As_2O_3$: MoO_3 glass ceramic network structure is considered to be build up from, SbO_3, $Sb^{v}O_4$, AsO_3 , PbO_4 and MoO_4^{2-} structural units that are linked together by Sb-O-Pb and Pb-O-As, Sb-O-As, Mo-O-As and Mo-O-Sb bonds.

A slight increase in the density of $PbO\text{-}Sb_2O_3\text{-}As_2O_3$: MoO_3 glass-ceramics has been observed with respect to that of corresponding glass samples (Table 3.2). In general, the structural compactness, the modification of the geometrical configuration of the glassy network, the change in the coordination of the glass forming ions and the fluctuations in the dimensions of the interstitial holes are the factors that influence the density of the glass-

ceramic material. The progressive introduction of crystallizing agent MoO_3 caused a slight decrease in the density; this is an indicative of decreasing structural compactness of the material. It is also an evocative of the increasing presence of molybdenum ions in Mo^{5+} state whose field strength is lower (when compared with that of Mo^{6+} state) that makes the sample less compact. The decreasing concentration of Sb^{5+} ions may also be responsible for such reduction in the density.

X-ray diffraction pattern of these samples exhibit micro-structural changes. The crystalline $Pb_5Sb_2O_8$, $PbSb_2O_6$, $SbAsO_4$, Sb_2MoO_6, $As_4Mo_3O_{15}$, $Pb_5Sb_4O_{11}$ seemed to be the main products in the present glass ceramic samples as mentioned earlier. In molybdenum rich glasses, the presence of $Sb_4Mo_{10}O_{31}$ crystalline phases are also detected. These meta stable crystals are usually in solid-solution phases that contain the major constituents of the glass composition in the approximately same proportion as they were present in the original glass matrix. This type of separation of various phases may lead to a Mo fortification of the droplet, leaving the glass matrix with a very low content of molybdenum. The Mo rich areas in the glass may enhance the reactivity of Mo with the other oxides that precipitate as high density of fine Mo rich crystals. These tiny crystals act as heterogeneous nuclei for the crystallization of the remaining glass. The scanning electron microscopic

pictures of glasses crystallized with MoO_3 exhibit larger crystals than those visible in the MoO_3 free samples. As the concentration of the MoO_3 increased, an increase in the degree of crystallinity with reasonably homogeneous distribution of the crystals can be seen. The residual glass phase may act as interconnecting zones among the crystallized areas making the samples free of voids and cracks. The crystalline phases viz., $PbSb_2O_6$, $SbAsO_4$ seem to be disappear as the content of the crystallizing agent is increased; this observation indicates that the concentration of Sb^{5+} ions is marginal in the samples crystallized with higher concentration of MoO_3. The average diameter 'd_c' of the induced crystal phases is evaluated using Scherrer's formula:

$$d_c = \frac{0.9\lambda}{\Delta\theta\cos\theta}, \qquad (3.3)$$

where λ is the wavelength of X-rays, $\Delta\theta$ is the half width of the diffraction peak; the average diameter of various crystalline phases evaluated using this formula found to be in the range of 20 to 50 nm. This diameter range is sufficiently far away from the wavelengths of the visible and NIR regions. In view of this, the scattering losses due to the difference of the refractive indices between crystallites and glass ceramic are expected to be negligibly small. Probably for this reason, these samples retain transparency even after the crystallization.

The DTA studies indicated that with increase in the concentration of nucleating agent MoO_3, the glass transition temperature T_g and the parameter T_C-T_g have been observed to decrease. The decrease in the augmented cross-link density of various structural groups and the reduction in the closeness of packing are responsible for such decrease of these parameters. The appearance of different crystallization temperatures in the DTA pattern obviously suggests the presence of different phases of crystallization in the samples. The resolution of endothermic peaks could not be observed in the DTA traces of the samples crystallized with higher concentration of the nucleating agent; this overlapping indicates the closeness of these peaks due to different crystalline phases. The crystallization in the samples may take place based on the surface and bulk nucleations. The non-isothermal devitrification process is represented by the Eq. [61],

$$\ln\left(\frac{1}{1-\alpha}\right) = \frac{AN}{\beta^n} e^{-\left(\frac{nE}{RT}\right)} \qquad (3.4)$$

where α is the fraction of the volume crystallized at temperature T, E is the activation energy and β is the DTA heating rate and A is the constant. The nuclei centers N are the sum of surface and bulk nuclei. The higher the value of N, the lower is the crystallization temperature T_c. In the surface nucleation mechanism, the nucleating centers are formed only on the surface and the

crystals start developing from the surface to the inside of the glass one dimensionally (in this case n = 1). On the other hand in bulk nucleation the crystals grow three dimensionally (in this case n = 3). The general shape of the crystallization peaks is strongly dependent with the value of n. The higher the value of n the narrower is the width of the crystallization peak [62]. For the surface crystallization we may therefore expect relatively wider peaks when compared with the peaks due to bulk crystallization. The pattern of the DTA peaks suggests the crystallization is predominantly due to the surface crystallization as the concentration of the crystallizing agent is increased.

The pragmatic decrease in the intensity of the bands due to symmetric stretching and bending vibrations of AsO_3 and SbO_3 structural units in the IR spectra with increase in the concentration of the crystallizing agent MoO_3 clearly suggests an increasing modifying action of molybdenum ions. As mentioned earlier an increase in the concentration of MoO_3 as crystallizing agent, there is a growing concentration of Mo^{5+} ions that take part modifying positions at the expense of Mo^{6+} ions that take part in network forming positions with MoO_4^{2-} tetrahedral units.

The band due to ν_1 vibrational mode of MoO_4^{2-} tetrahedral units located at about 890 cm^{-1} (in the spectrum of glass ceramic M_2) is observed

to be shifted towards a region of higher wavenumber (902 cm^{-1}); in this region the band due to partially isolated Mo-O bonds of the strongly deformed MoO_6 groups is expected [63]. Similarly the ν_3 vibrational band of MoO_4^{2-} units observed at about 835 cm^{-1} in the spectrum of glass M_2 is shifted towards (lower wavenumber) the region of antisymmetric stretching vibrations of a Mo-$_{short}O_{long}$-Mo bridge associated with MoO_6 octahedra containing Mo=O bond [64]. These results thus confirm a gradual transformation of molybdenum ions from tetrahedral positions to octahedral positions with increase in the concentration of crystallizing agent MoO_3.

Broad absorption band observed in the region of 670-690 nm in the optical absorption spectra of these glass ceramics is attributed to the excitation of Mo^{5+} ($4d^1$) ion. In fact, for this ion, two optical excitations were predicted starting from $b_2(d_{xy})$ ground state to (d_{xz-yz}) and ($d_{x^2-y^2}$) with E_1=15000 cm^{-1} and E_2=23000 cm^{-1} [65]. Perhaps, due to inter charge transition transfer ($Mo^{5+} \Leftrightarrow Mo^{6+}$) in the glass network, the resolution of these transitions could not be observed. The optical activation energy has been found to be of about 1.70–1.85 eV for the investigated glass ceramic samples, and this is clearly a characteristic signal of inter valence transfer or a polaronic type of absorption.

The inset of Fig. 3.7 (and Table 3.4) shows that the peak energy, decreases considerably with increase in the concentration of nucleating agent; this observation clearly indicates that the associated electrons are still trapped at shallow sites within the main band gap and yet have smaller wave-function radii. In terms of polaronic perception, this kind of situation is only possible if the local potential fluctuation is small as compared to the transfer integral, j. A small overlap between electronic wave functions (corresponding to adjacent sites) due to strong disorder is contributive to polaron formation. So from the polaronic viewpoint, the electron delivered by the impurity atom at the Mo^{6+} site converts this into a lower valence state Mo^{5+}, and at the next stage, the trapped electron at this Mo^{5+} site is transferred to the neighboring new Mo^{6+} site by absorbing a photon energy. Thus the optical absorption in the glass ceramic samples is dominated by polaronic transfer between the Mo^{5+} and Mo^{6+} species depending upon the state of coloration, i.e., when the samples develop into dark brown or turn into blue coloration [26, 66].

The increasing intensity of this band with increase in the concentration of crystallizing agent suggests the growing presence of Mo^{5+} ions in the glass ceramic samples. Such Mo^{5+} ions may form $Mo^{5+}O_3^-$ molecular orbital states and are expected to participate in the depolymerisation of the glass network

and create more bonding defects and non-bridging oxygens (NBO's). The higher the concentration of such modifiers, the higher is the concentration of NBO's in the glass matrix. This leads to increase in the degree of localization of electrons there by increasing the donor centres in the glass matrix. The presence of higher concentration of these donor centers decreases the optical band gap and shifts the absorption edge towards higher wavelength side as observed. In the polaronic perspective, the nucleating agent concentration change in the band gap can be explained as follows. With the increase in concentration of Mo^{5+} ions, a large number of donor centers are created, and subsequently, the excited states of localized electrons originally trapped on Mo^{5+} sites begin to overlap with the empty 4d states on the neighboring Mo^{6+} sites, and as a result, the impurity or polaron band becomes more extended into the main band gap. This new polaronic development might have shifted the absorption edge to the lower energy (Table 3.3) which leads up to a significant shrinkage in the band gap.

The magnetic properties of these glasses arise due to Mo^{5+} ($4d^1$) paramagnetic ions. The increase in the value of redox ratio C (obtained from magnetic susceptibility measurements), with increase in the concentration of crystallizing agent MoO_3, indicates a gradual increase in the reduction of molybdenum ions from Mo^{6+} state to Mo^{5+} state in the glass matrix.

The ESR spectrum of $PbO\text{-}Sb_2O_3\text{-}As_2O_3$: MoO_3 glass-ceramics consists of a main central line surrounded by less intense satellites. The central line arises from even molybdenum isotopes (I = 0) whereas satellite lines correspond to the hyper fine structure from odd ^{95}Mo and ^{97}Mo (I = 5/2) isotopes [25, 65]. The highest intensity of the signal observed in the spectrum of the sample M_{10}, suggests the presence of the highest concentration of $Mo^{5+}O_3^-$ complexes. The values of $g_\perp$ and g_{ll} from this spectrum have been found to be dependant on the concentration of crystallizing agent; the structural disorder arising from the site-to-site fluctuations of the local surroundings of the paramagnetic Mo^{5+} ions can be accounted for such variations. The variation of MoO_3 content has considerably affected the intensity of the signal; in fact the signal is observed to be feeble for the samples crystallized with lower concentration of MoO_3. The g values obtained for these glasses are found to be consistent with the reported values for many other glass and glass ceramic systems containing molybdenum ions [67-70].

The intensity and the half width $\Delta B_{1/2}$ of the signal is found to increase with increase in the concentration of the crystallizing agent. For dipolar interactions between paramagnetic ions, the half-width (in Tesla) of the signal is given by [71],

$$2\Delta B_{1/2} = 3.62 \frac{\mu_O}{4\pi} \frac{(g_{\perp}^2 + 2g_{\text{II}}^2)}{g} \frac{\beta}{d^3} C \quad ; \qquad (3.5)$$

here, g is the mean g-value. From this equation, we have calculated the minimal distance d between two molybdenum ions, (with the C being the value of reduction factor) and presented in Table 3.4; these distances are observed to be far greater than the Mo-O-Mo distance in several compounds [72]. From these data, we conclude that the molybdenum containing structural units in these glass ceramics can only share edges or faces and not common corners [71].

The analysis of ESR spectra of these samples further suggest that Mo^{5+} ions are essentially coordinated in these glass ceramics by five oxygen ligands in a square pyramidal form C_{4v} symmetry with a Mo=O double bond [73]. The degree of axial distortion α of the coordination polyhedron [74] is evaluated using Eq.

$$\alpha = \frac{g_e - g_{ll}}{4(g_e - g_{\perp})} ; \qquad (3.6)$$

the value of α is found to increase considerably with increase in the content of MoO_3 (inset (b) of Fig. 3.9). Such an observation indicates that the oxygen atoms surrounding the molybdenum progressively become non-bridging and

non-equivalent, resulting in a decrease in symmetry or increasing disorder in the glass ceramic samples.

In the case of a distorted octahedral environment of the paramagnetic ion, the short-range disorder can be described by the ratio

$$\frac{\Delta R}{R} = \frac{2}{5}\frac{\Delta g_{ll}}{g_e - g_{ll}} \qquad (3.7)$$

where R is the average length of Mo-O bond and Δg_{ll} is the r.m.s. deviation of g_{ll}. The average value of $\Delta R/R$ obtained for these samples ~2 % indicating that short-range order is still preserved in these glass ceramic samples [75].

With the gradual increase of the crystallizing agent MoO_3 from 0 to 1.0 mol%, the values of the dielectric parameters viz., ε', tan δ and σ_{ac} are found to increase at any frequency and temperature and activation energy for a.c. conduction is observed to decrease with respect to those of pre-crystallized samples; this is an indication of an increase in the space charge polarization. Such increase is vividly due to the growing presence of Mo^{5+} ions that act as modifiers in these samples. Normally, the modifying ions generate bonding defects in the glass network as mentioned before; the defects thus produced create easy path ways for the migration of charges that would build up space charge polarization and facilitate to an increase in the dielectric parameters as observed [76-78].

Further support for the increasing concentration of Mo^{5+} ions with increasing content of the nucleating agent can also be cited from the relaxation effects of dielectric loss. Earlier studies on the glasses containing d^1 ions like W^{5+}, Cr^{5+}, V^{4+}, Ti^{3+} showed that these ions contribute to the dielectric relaxation effects [79-81]. Hence the relaxation effects observed in the present glass ceramics are obviously due to Mo^{5+}. The gradual increase in the breadth and the intensity of the relaxation peaks and the decrease in the activation energy for dipoles indicate a gradual increase in the concentration of $Mo^{5+}O^{-}_{3}$ ions with increase in the concentration of nucleating agent; this fact is also evidenced from optical absorption and ESR spectra. The presence of such molybdenum complexes may increase the concentration of ruffled Sb-O-Pb and Pb-O-As, Sb-O-As, Mo-O-As Mo-O-Sb etc. bonds in the glass ceramic network and decreases the rigidity; such a loosely packed network offers more freedom for dipoles to orient in the field direction and decrease the activation energy for dipoles as observed (Table 3.5).

When a plot is made between log $\sigma(\omega)$ vs. activation energy for conduction (in the high temperature region) a near linear relationship is observed (inset (a) of Fig. 3.13); this observation suggests that the conductivity enhancement is directly related to the thermally stimulated mobility of the charge carriers in the high temperature region. The values of

the thermal-activation energy of the reported data have been gauged in the range 0.2–0.4 eV, this range still covers the semiconducting behaviour of glass ceramics.

The conductivity isotherm as a function of the concentration of crystallizing agent MoO_3 exhibit a slow increase for low concentration of crystallizing agent and a steep increase is observed when the concentration of MoO_3 is greater than nearly 0.5 mol%. With the entry of Sb^{5+} ions in to the glass network, the electronic paths may be blocked causing an inhibition of the electronic current. The mobile electrons, or polarons, involved in the process of transfer from Mo^{5+} to Mo^{6+} are attracted by the oppositely charged positive ions. This cation-polaron pair moves together as a neutral entity. As expected, the migration of this pair is not associated with any net displacement of the charge and thus does not contribute to electrical conductivity, as a result, a slow increase in the conductivity results.

The low temperature part of the conductivity (a near temperature independent part, as in the case of present glasses up to nearly 350 K) can be explained on the basis of quantum mechanical model [82]. The equation for a.c. conductivity due to quantum mechanical tunneling is given by [82]:

$$\sigma(\omega) = \eta e^2 KT\left[NE_F\right]^2 \ \alpha^{-5} \ \omega\left[\ln\frac{\nu_{ph}}{\omega}\right]^4 \qquad (3.8)$$

From eqn. (6), the value of $N(E_F)$, i.e. the density of the defect energy states near the Fermi level is evaluated, taking the value of α (electronic wave function decay constant) as 0.48 (A°) (obtained by plotting log σ_{ac} against R_i) and ν_{ph} the phonon frequency ($5x10^{12}$ Hz) and η is a constant and its value is given by $\eta = \pi/3$ (Austin & Mott [82]), $= 3.66\pi^2/6$ (Butcher & Hyden [83]), $= \pi^4/96$ (Pollak [84]) is computed for a frequency of 10^5 Hz at T=323 K and presented in Table 3.6. The value of $N(E_F)$ is found to increase with increase in the concentration of MoO_3. Such increase also suggests an increasing disorder in the glass ceramic network with increase in the concentration of nucleating agent MoO_3.

3.6 Conclusions

Molybdenum ions could successfully be used as strong nucleating agents for inducing various crystalline phases in $PbO\text{-}Sb_2O_3\text{-}As_2O_3$ glass samples. XRD and SEM studies clearly revealed the presence of various crystalline phases in these glass ceramic samples. The EDS analysis indicated the retention of all the elements in these samples even after crystallization. These studies further indicated the uniform distribution of the nucleating agents in the bulk glass ceramic samples. The approximate dimensions of various crystal phases evaluated from XRD data indicate that the size of the microcrystals is such that scattering loss in the visible and NIR

regions in these glass ceramic samples is negligibly small.. The differential thermal analysis studies pointed out that the surface crystallization prevails over the bulk crystallization as the concentration of the crystallizing agent is increased. The optical absorption spectra of $PbO\text{-}Sb_2O_3\text{-}As_2O_3$: MoO_3 glass-ceramics exhibit a broad band due to the transitions of Mo^{5+} ions, indicating the existence of molybdenum ions in pentavalent state, in addition to hexavalent state in these samples. The analysis of ESR spectra of these samples further suggested that Mo^{5+} ions are essentially coordinated in these glass ceramics by five oxygen ligands in a square pyramidal form C_{4v} symmetry with a Mo=O double bond. The magnetic susceptibility studies on these glass ceramics indicated an increase in the redox ratio with increase in the concentration of nucleating agent. The analysis of the dielectric properties suggested an increasing semiconducting character with increase in the concentration of the crystallizing agent.

References

1. P. W. McMillan, "*Glass-Ceramics," 2nd ed*. (Academic Press, London, 1979).

2. A.F. Wells, *Structural Inorganic Chemistry*, Oxford: Clarendon Press (1984).

3. F. F. Ferreira, T. G. S. Cruz, M. C. A. Fantini, M. H. Tabacniks, S. C. de Castro, J. Morais, A. de Siervo, R.Landers, A. Gorenstein, *Solid State Ionics* 357 (2000) 136.

4. Y. Dimitriev, J.C.J. Bart, V. Dimitrov, M. Arnaudov, Z. Anorg, *Allg. Chem.* 479 (1981) 229.

5. Y. Dimitriev, V. Dimitrov, M. Arnaudov, *J. Mater. Sci.* 18 (1983) 1353.

6. I.R. Beattie, T.R. Gilson, *Proc. Royal. Soc. (London). A* 307 (1968) 407.

7. I.R. Beattie, T.R. Gilson, *J. Chem. Soc. (A*) (1969) 2322.

8. K.S. Sidhu, Sukhprt Singh, S.S. Sekhon, S. Chandra, A. Kumar, *Phys. Chem. Glasses* 32 (1991) 255.

9. A.A. Bhagat, M.M. El-Samanoudy, *J. Phys. Chem. Solids* 60 (1999) 1921.

10. R. Mattes, F. Schroder, *Z. Naturforsch* 24b (1969) 1095.

11. D. Klissurski, Y. Pesheva, N. Abadjeva, *Appl. Catal*. 77 (1991) 55.

12. M. Pal, K. Hirota, H. Sakata, *J. Appl. Phys*. 34 (2001) 459.

13. A.M-Milankovic, A.Gajovic, D.E.Day, *J.Non-Cryst. Solids* 325 (2003) 76.

14. S. Simon, A.C. Nicula, *J. Non-Cryst. Solids* 57 (1983) 23.

15. J.F. Lyneh, S.L. Segel, G. Rosenblatt, *J. Appl. Phys*. 42 (1971) 2587.

16. B. Bridge, N.D. Patel, *J. Non-Cryst. Solids* 91 (1987) 27.

17. K.J. Rao, G. Pathasarathy, U. Selvaraj, E.S.R. Gopal, *Phys. Chem. Glasses* 26 (1985) 101.

18. B.B. Das, R. Ambika, *Chem. Phys. Lett.* 370 (2003) 670.

19. S.H. Morgan, R.H. Magruder III, *J. Am. Ceram. Soc.* 73 (1990) 753.

20. B.V.R. Chowdari, P. P. Kumari, *Solid State Ionics* 113 (1998) 665.

21. M.M. Elkholy, R.A. El-Mallawany, *Mater. Chem. Phys*. 40 (1995) 163.

22. A. M-Milankovic, D.E. Day, *J. Non-Cryst. Solids* 330 (2003) 128.

23. G. Govindaraj, N. Baskaran, K. Shahi, *Solid State Ionics* 76 (1995) 47.

24. L. Srinivasa Rao, M. Srinivasa Reddy, D. Krishna Rao, N. Veeraiah, *J. Solid State Sci.* 11 (2009) 578.

25. O. Cozar, D.A. Magdas, I. Ardelean, *J. Non-Cryst. Solids* 354 (2008) 1032.

26. Z. Hussain, *J. Electronic Mater*. 31 (2002) 615.

27. Yasser B Saddeek, A M Abousehly and Shaban I Hussien, *J. Phys. D: Appl. Phys*. 40 (2007) 4674

28. Naoaki Kuwata, Taira Saito, Masahiro Tatsumisago, Tsutomu Minami and Junichi Kawamura, *J Non-Cryst. Solids* 324 (2003) 79.

29. Silvia H. Santagneli, Carla C. de Araujo, Wenzel Strojek, and Hellmut Eckert, *J. Phys. Chem. B* 111 ((2007) 10109

30. S. Hemlata, P.R. Sarode, K.J. Rao, *J. Non-Cryst. Solids* 54 (2009) 313.

31. A.M. Al-Shukri, G.D. Khattak, M.A. Salim, *J. Mater. Sci.* 35 (2000) 123.

32. M. El-Hofy, I.Z. Hager, *Phys. Stat. Solidi (a)* 182 (2000) 697

33. Jose, Rajan; Arai, Yusuke; Ohishi, Yasutake, *Appl. Phys. Lett.* 93 (2008) 161901

34. Chung, Woon Jin; Park, Bong Je; Seo, Hong Seok; Ahn, Joon Tae; Choi, Yong Gyu, *Eur. J. Glass Sci. Tech.* 50 (2009) 113.

35. R. Iordanova, V. Dimitrov, D. Klissurski, *J. Non-Cryst. Solids* 180 (1994) 58.

36. T.Sekiya, N. Mochida, S. Ogawa, *J. Non-Cryst. Solids* 185 (1995) 135.

37. M.Jamniky, P. Znasik, M.D. Ingram, *J. Non-Cryst. Solids* 185 (1995) 151.

38. D. Boudlich, M. Haddad, J. Kliava, *J. Non-Cryst. Solids* 224 (1998) 151.

39. M. El-Hofy, I.Z. Hager, *Phys. Stat. Solidi (a)* 182 (2000) 697.

40. N. Machida, *Solid State Ionics* 107 (1998) 255.

41. L. Bih, El Omari, M.Haddad, *Mater. Lett.* 50 (2001)308.

42. S. Muthupari, K.J. Rao, *J. Phys. Chem. Solids* 57 (1996) 553.

43. H.H. Qiu, M. Kudo, H. Sakata, *Mater. Chem. Phys.* 51 (1997) 233.

44. M.D. Ingram, A.J. Pappin, *Phys. Chem. Glasses* 32 (1991) 121.

45. G.D. Khattak, M.A. Salim, L.E.Wenger, *J. Non-Cryst. Solids* 212 (1997) 180.

46. Powder Diffraction File, Alphabetical Index, Inorganic Compounds 2003, Published by JCPDS – International Centre for Diffraction Data, Newtown Square, PA. 19073-3273

47. A. Bishay, C. Maghrabi, *Phys. Chem. Glasses* 10 (1969) 1.

48. B. Dubois, J.J. Videau, M. Couzi, J. Portier, *J. Non-Cryst. Solids* 88 (1986) 355.

49. P. Subbalakshmi, P.S. Sastry, N. Veeraiah, *Phys. Chem. Glasses* 42 (2001) 307.

50. N. Machida, H. Eckert, *Solid State Ionics* 107 (1998) 255.

51. S.R. Elliott, *Phys. Amor. Mater.* (Longmann Sci., Essex, 1990).

52. K. Muruganandam, M. Seshasayee, *Phys. Chem. Glasses* 40 (1999) 287.

53. Bing Zhang, Qi Chen, Li Song, Huiping Li, Fengzhen Hou, Jinchao Zhang, *J. Non-Cryst. Solids* 354 (2008) 1948

54. P.J. Miller, C.A. Cody, *Spectrodum Acta Cryst. A* 38 (1982) 555.

55. M. Srinivasa Reddy, S.V.G.V.A. Prasad, and N. Veeraiah, *Phys. Stat. Solidi (a),* 204 (2007) 816

56. J.J. Kleperis, P.D. Cikmach, A.R. Lusis, *Phys. Stat. Solidi (a)* 83 (1984) 291.

57. Y.R. Zakis, A.R. Lusis, Y.R. Lagzduns, *J. Non-Cryst. Solids* 47 (1982) 267.

58. D. Holland, *Solid State NMR* 26 (2004) 72

59. K.V. Damodaran and K.J. Rao, *Chem. Phys. Lett*. 148 (1988) 57.

60. M. Srinivasa Reddy, V.L.N. Sridhar Raja and N. Veeraiah, *EPJ Appl. Phys.* 37 (2007) 203; P. Syam Prasad, M. Srinivasa Reddy, V. Ravi Kumar and N. Veeraiah, *Philos. Mag.* 87 (2007) 5763.

61. K. Matusita, S. Sakka, *Bull. Inst. Chem. Res*., Kyoto Univ., 59 (1981) 159.

62. A. Marotta, A. Buri, F. Branda, *J. Mater. Sci.,* 16 (1981) 341.

63. R Iordanova, Y Dimitriev, V. Dimitrov, S. Kassabov, D. Klissurski, *J. Non-Cryst. Solids* 231 (1998) 227

64. R. Iordanova, Y. Dimitriev, *J. Non-Cryst. Solids* 231 (1998) 227.

65. G. Srinivasarao, N. Veeraiah, *J. Solid State Chem*. 166 (2002) 104.

66. G. Calas, M.Le Grand, L.Galoisy, D. Ghaleb, *J. Nuclear Mater*. 322 (2003) 15.

67. B.V. R. Chowdari, K. Radha Krishnan. *J. Non-Cryst. Solids* 224 (1998) 151.

68. M. Haddad, A. Nadiri, A. Biyadi, M.E. Archidi, J.V. Folgado, D. Beltran-Porter, *J. Alloys Compd.* 188 (1992) 161.

69. B.B. Das, R. Ambika, *Chem. Phys. Lett.*370 (2003) 670.

70. P. Syamprasad, B.V. Raghavaiah, R. Balaji rao, C. Laxmikanth, N. Veeraiah, *J. Solid State Commun.* 132 (2004) 235.

71. R. Berger, J. Kliava, P. Beziade, *J. Non- Cryst. Solids* 180 (1995) 151.

72. H.J. Wagner, P. Drissen, C.F. Schwerdtfeger, *J. Non-Cryst. Solids* 34 (1971) 1335.

73. D. Boudlich, M. Haddad, A. Nadiri, R. Berger, J. Kliava, *J. Non-Cryst. Solids* 224 (1998) 135.

74. R. Berger, P. Beziade, A. Levasseur, Y. Servant, *Phys. Chem. Glasses* 31 (1990) 231.

75. A. Bals, J. Kliava, *J. Magn. Reson*. 53 (1983) 243; *J. Phys.: Condens. Matter* 3 (1991) 6209.

76. G. Murali Krishna, M. Srinivasa Reddy and N. Veeraiah, *J. Solid State Chem.* 180 (2007) 2747.

77. P. Venkateswara Rao, T. Satyanarayana, M. Srinivasa Reddy, Y. Gandhi and N. Veeraiah, *Physica B* 403 (2008) 3751

78. K. Sambasiva Rao, M. Srinivasa Reddy, V. Ravi Kumar and N. Veeraiah, *Mater. Chem. Phys.* 111 (2008) 283

79. R.M. Abdelouhab, R. Braunstein, K. Baerner, *J. Non-Cryst. Solids* 108 (1989) 109.

80. L. Srinivasa Rao, M. Srinivasa Reddy, M. Rami Reddy, N. Veeraiah, *J. Alloys Compd.* 464 (2008) 472

81. G. Murali Krishna, Y. Gandhi, N. Veeraiah, *Physica B* 403 (2008) 702.

82. I.G. Austin, N.F. Mott, *Adv. Phys.* 18 (1969) 657.

83. P. Butcher, K. Hyden, *Philos. Mag.* 36 (1977) 657.

84. M. Polak, *Philos. Mag.* 23 (1971) 519.